J. Condensed Matter Nucl. Sci. 22 (2017) 53–73

Research Article

Probabilistic Models for Beam, Spot, and Line Emission for Collimated X-ray Emission in the Karabut Experiment

Peter L. Hagelstein*

Massachusetts Institute of Technology, Cambridge, MA, USA

Abstract

Collimated X-ray emission near 1.5 keV in the Karabut experiment is an anomaly that cannot be explained by conventional solid state, atomic, or nuclear physics. In order for the X-rays to be collimated, there must either be an X-ray laser present, or else a phased-array collimation effect produced by emitting dipoles that radiate in phase. Although there have been arguments made in support of an X-ray laser origin of the effect, from our perspective this approach suffers from an absence of a plausible mechanism, short excited-state electronic lifetimes, high power requirements, and an incompatibility between the experimental geometry and the need for an elongated laser medium for beam formation. In this work we consider a model for beam formation due to many emitting dipoles randomly positioned within a circle on a mathematically flat surface. When the emitting dipole density is low, a speckle pattern is produced. Above a critical emitting dipole density beam formation occurs. The average intensity of the speckle and beam is estimated from simple statistical models at low and high dipole density, and combined to develop an empirical intensity estimate over the full range of dipole densities which compares well with numerical simulations. Beam formation occurs above a critical number of emitting dipoles, which allows us to develop an estimate for the minimum number of emitting dipoles present in the Karabut experiment. The effect of surface deformations is considered; constant offsets do not impact beam formation, and locally linear offsets direct the beam slightly off of normal. Minor displacements quadratic in the surface coordinates can produce focusing and defocusing effects, leading to a natural explanation for intense spot and line formation observed in the experiments.
 ISSN 2227-3123

Keywords: Beam formation, Collimated X-ray emission, Karabut experiment, Phase coherence, Up-conversion

1. Introduction

Karabut and his coworkers at the Luch Institute reported the observation of excess heat and other anomalies in glow discharge experiments in the early 1990s [1]. In subsequent experiments Karabut noticed that soft X-rays near 1.5 keV were emitted, and that they were collimated upward in his experiment normal to the cathode surface [2]. This effect was studied for more than a decade [3–10], and was found to be independent of the cathode metal (the effect was seen with Al, and with other metals through W), also to be independent of which discharge gas was used (collimated emission was seen with H_2, D_2, He, Ne, Ar and Xe).

*E-mail: plh@mit.edu

 ISSN 2227-3123

Collimated X-ray emission in this experiment is a striking anomaly for a variety of reasons. In order to arrange for collimated X-ray emission, either you need an X-ray laser, or else you need coherence among the emitter phases; either option would have deep implications. Karabut was convinced, especially in his later years, that he had made an X-ray laser. In some recent articles Ivlev speculates about the possibility of an X-ray laser mechanism in connection with Karabut's experiment [11,12].

In years past the author spent a decade modeling and designing X-ray lasers [13]; an experience that led to an understanding of just how difficult it is to create a relevant population inversion and to amplify X-rays. The notion of a population inversion at 1.5 keV involving electronic transitions in a solid state environment is unthinkable due to the very short lifetime. And then even if somehow a population inversion could be generated, one would need enough amplifier length to produce a collimated beam (the solid state medium is very lossy), as well as an amplifier geometry consistent with the observed beam formation. The very broad line shape associated with the collimated emission also argues against an X-ray laser mechanism. All of these headaches combine to rule out an X-ray laser mechanism associated with the solid. The primary headache associated with an X-ray laser in the gas phase is the absence of relevant electronic transitions in hydrogen, deuterium, helium and in neon gas. In this case one could contemplate the possibility of a ubiquitous impurity in the discharge gas; however, this leads to an additional headache of coming up with enough inverted atoms, molecules or ions to provide many gain lengths. If somehow one has any optimism left for the approach, a consideration of the relatively long (millisecond) duration of the collimated X-ray emission following the turning off of the discharge current should provide a cure. If the upper state radiative life time is long then the gain is very low; and if the gain is high then the upper state radiative life time is very short and the power requirement becomes prohibitive.

All of these arguments have led us to consider collimated X-ray emission as a result of a phased array emission effect. In this case serious issues remain; such as how excitation is produced (which in this case is much easier since a population inversion is not required); and how phase coherence might be established. From our perspective, both excitation and phase coherence could be developed via the up-conversion of vibrations to produce nuclear excitation in ^{201}Hg, which is special because it has the lowest energy excited state (at 1565 eV) of any of the stable nuclei. We have reported on our earlier studies of models that describe up-conversion in the lossy spin-boson model, and various extensions and generalizations [14–16].

In this work we consider models for beam formation of the collimated X-ray emission in Karabut's experiment based on the assumption of phase coherent emitting dipoles randomly positioned on a plane, in connection with the "diffuse" X-ray emission effect observed under "normal" high-current operating conditions. The collimated X-rays in this case were observed to be normal to the cathode in a beam essentially the same size as the cathode; we find that beam formation in the high dipole density of the model (where the emission is produced from localized dipoles) works the same way. When the emitting dipole density is low then no beam forms, but a speckle pattern is produced. It might be proposed that the very intense spots seen in the experiments following the turning off of the discharge are connected with the random constructive interference effects that lead to speckle. However, we find that individual spots associated with the speckle pattern are too small to account for this "sharp" emission effect, and that speckle cannot account for lines or curves. Instead we find that spot formation and line formation follow naturally from models that describe surface deformations that are quadratic or higher-order in the transverse surface coordinates.

A weak speckle pattern is generated at low emitting dipole density, and a beam is produced when the emitting dipole density is high. A critical number or density of emitting dipoles can be estimated for the development of a beam. Since beam formation is reported in Karabut's experiment, it is possible to develop a constraint on the number of emitting dipoles consistent with experiment. We have conjectured previously that a small amount of mercury contamination in the chamber might result in some mercury sputtered onto the cathode surface, resulting in a relatively small number of mercury nuclei that emit on a broadened version of the 1565 eV transition in ^{201}Hg. It is possible to develop a lower

bound on the number of mercury atoms present near the surface, to see whether it is consistent with the proposed picture.

Key features of the model which allows for collimation of the emitted beam normal to the surface are the phase coherence assumed, as well as the surface itself (which in the model is mathematically flat). There is no reason to think that the cathode surface is flat at the atomic scale, since whatever the surface looked like initially is modified in the ion bombardment, and surface loss through sputtering, which occurs during discharge operation at high current density. Mercury atoms in the discharge gas ionized above the cathode fall would be accelerated toward the cathode surface in this picture with an energy of up to a few keV, which means that they would end up randomly positioned in the outer 5–10 nm of the cathode surface. If so, then one would not expect any alignment in a plane, as assumed in the model, unless there were an ordering of the crystal planes so that some fraction of them were aligned with the cathode surface. The expected randomization of the locations of the mercury atoms inside the cathode surface would make beam formation to be impossible, except from the occasional crystal plane accidentally aligned with the surface.

However, it is well known in the literature that substantial deformation of a metal, as occurs during rolling, can result in a substantial alignment of the local crystal planes with the surface [17–19]. It seems likely that the cathodes used by Karabut were from stock that was rolled, so that one would expect the cathodes themselves to provide a source of crystal planes oriented with the surface. During the discharge operation the cathodes undergo additional surface deformation due to local thermal effects and electrostatic forces, which provides a natural mechanism for intense spot and line formation. In this picture the crystal ordering built in during rolling is largely maintained during the deformations that occuring during discharge operation.

2. Basic Model

We note that models for random arrays of emitting dipoles have been studied previously; in the case of random linear arrays, see [20–23]; a model for a random distribution of antennas in a two dimensional circle has been studied in [24]; and for a random distribution in a triangle in [25]. Statistical models for the analysis of beam formation from random antenna arrays have also been discussed in [26–28].

Following the discussion above, we turn our attention to a simple model for X-ray emission due to a collection of identical emitting dipoles that are randomly distributed in a plane. We can write for the vector potential in the case of oscillating electric dipoles [29] the summation

$$\mathbf{A}(\mathbf{r}) = -i\sum_j \frac{k\mathbf{p}_j}{|\mathbf{r}-\mathbf{r}_j|}\exp\left\{ik|\mathbf{r}-\mathbf{r}_j|\right\} \rightarrow -i\frac{k\mathbf{p}}{|\mathbf{r}|}\sum_j \exp\left\{ik|\mathbf{r}-\mathbf{r}_j|\right\}, \tag{1}$$

where we have assumed uniform phase, identical dipoles, and we focus on the field that results far away from the plane. The nuclear transition in ^{201}Hg is a magnetic dipole transition, which provides the motivation to consider the analogous approximation for a set of oscillating magnetic dipoles

$$\mathbf{A}(\mathbf{r}) = i\sum_j \frac{k\hat{\mathbf{n}}_j\times\mathbf{m}_j}{|\mathbf{r}-\mathbf{r}_j|}\exp\left\{ik|\mathbf{r}-\mathbf{r}_j|\right\} \rightarrow i\frac{k\hat{\mathbf{n}}\times\mathbf{m}}{|\mathbf{r}|}\sum_j \exp\left\{ik|\mathbf{r}-\mathbf{r}_j|\right\}. \tag{2}$$

In either case, the resulting intensity is proportional to

$$I(\mathbf{r}) \sim \left|\sum_j \exp\left\{ik|\mathbf{r}-\mathbf{r}_j|\right\}\right|^2 = \sum_j\sum_{j'}\exp\left\{ik(|\mathbf{r}-\mathbf{r}_j|-|\mathbf{r}-\mathbf{r}_{j'}|)\right\}. \tag{3}$$

The dipoles are assumed to lie in the emitting plane defined by $z_j = 0$, and we are interested in the intensity pattern produced at image plane defined by $z = Z$ (a schematic is shown in Fig. 1). In this case we can write

$$I(x,y,Z) \sim \sum_j \sum_{j'} \exp\left\{ik\left(\sqrt{(x-x_j)^2+(y-y_j)^2+Z^2} - \sqrt{(x-x_{j'})^2+(y-y_{j'})^2+Z^2}\right)\right\}. \quad (4)$$

Simulations based on this model predicts beam formation for small areas when the dipole density is high, and spot formation in the case of larger areas or when the dipole density is low.

Since the locations of the dipoles are probabilistic, it will be of interest to estimate the expectation value of the intensity

$$\mathrm{E}[I(\mathbf{r})] \sim \sum_j \sum_{j'} \mathrm{E}\left[\exp\left\{ik(|\mathbf{r}-\mathbf{r}_j| - |\mathbf{r}-\mathbf{r}_{j'}|)\right\}\right]. \quad (5)$$

In what follows we will focus on specific model results for the summation on the right-hand side.

3. Beam Formation in the High Density Limit

Beam formation occurs when there are several dipoles that are sufficiently close together so that their contributions can combine coherently. In this regime there is the possibility of making use of a Taylor series expansion according to

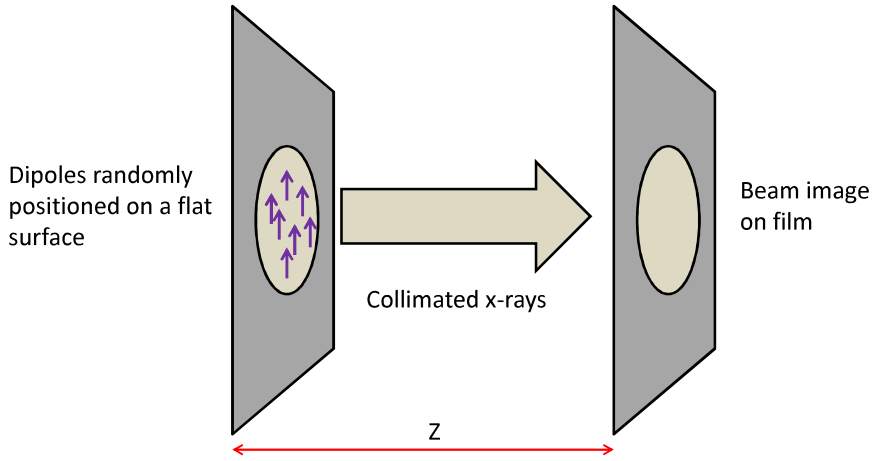

Figure 1. Schematic of the model. Phase coherent dipoles are positioned randomly within an emitting area of the cathodes surface, and radiate to form a beam if the emitting dipoles are in phase and have a sufficiently high density.

$$
\begin{aligned}
|\mathbf{r}-\mathbf{r}_j| &= \sqrt{(x-x_j)^2+(y-y_j)^2+Z^2} \\
&= Z\sqrt{1+\frac{(x-x_j)^2}{Z^2}+\frac{(y-y_j)^2}{Z^2}} \\
&= Z\left[1+\frac{(x-x_j)^2}{2Z^2}+\frac{(y-y_j)^2}{2Z^2}+\cdots\right].
\end{aligned} \tag{6}
$$

In this case we can write for the difference

$$
\begin{aligned}
|\mathbf{r}-\mathbf{r}_j|-|\mathbf{r}-\mathbf{r}_{j'}| &= \frac{(x-x_j)^2}{2Z}+\frac{(y-y_j)^2}{2Z}-\frac{(x-x_{j'})^2}{2Z}-\frac{(y-y_{j'})^2}{2Z}+\cdots \\
&= \frac{(x_{j'}-x_j)x+(y_{j'}-y_j)y}{Z}+\frac{x_j^2-x_{j'}^2+y_j^2-y_{j'}^2}{2Z}+\cdots
\end{aligned} \tag{7}
$$

If we assume that beam formation is dominated by contributions from the lowest order terms in the Taylor series expansion, then we can write

$$
I(x,y,Z)\sim\sum_j\sum_{j'}\exp\left\{ik\left(\frac{(x_{j'}-x_j)x+(y_{j'}-y_j)y}{Z}+\frac{x_j^2-x_{j'}^2+y_j^2-y_{j'}^2}{2Z}\right)\right\}. \tag{8}
$$

The locations of the emitting dipoles are random variables, so that the intensity will be random as well. It will be of interest to estimate the expectation value of the intensity which we can write as

$$
\mathrm{E}[I(x,y,Z)]\sim\sum_j\sum_{j'}\mathrm{E}\left[\exp\left\{ik\left(\frac{(x_{j'}-x_j)x+(y_{j'}-y_j)y}{Z}+\frac{x_j^2-x_{j'}^2+y_j^2-y_{j'}^2}{2Z}\right)\right\}\right]. \tag{9}
$$

If we assume that the various x_j and y_j values are independent, then this becomes

$$
\begin{aligned}
\mathrm{E}[I(x,y,Z)]\sim\sum_j\sum_{j'}&\mathrm{E}\left[\exp\left\{ik\left(\frac{-2x_jx+x_j^2}{2Z}\right)\right\}\right]\mathrm{E}\left[\exp\left\{-ik\left(\frac{2x_{j'}x+x_{j'}^2}{2Z}\right)\right\}\right], \\
&\mathrm{E}\left[\exp\left\{ik\left(\frac{-2y_jy+y_j^2}{2Z}\right)\right\}\right]\mathrm{E}\left[\exp\left\{-ik\left(\frac{2y_{j'}y+y_{j'}^2}{2Z}\right)\right\}\right] \\
&= N^2\left|\mathrm{E}\left[\exp\left\{ik\left(\frac{-2x_jx+x_j^2}{2Z}\right)\right\}\right]\mathrm{E}\left[\exp\left\{ik\left(\frac{-2y_jy+y_j^2}{2Z}\right)\right\}\right]\right|^2.
\end{aligned} \tag{10}
$$

For simplicity, let us assume uniform probability distributions for a square emitting region defined by

$$
\begin{aligned}
f_X(x_j) &= \frac{1}{L} \quad (-L/2<x<L/2), \\
f_Y(y_j) &= \frac{1}{L} \quad (-L/2<x<L/2).
\end{aligned} \tag{11}
$$

Also for simplicity let us focus on the origin at the image, so that

$$\mathrm{E}[I(0,0,Z)] \sim N^2 \left| \mathrm{E}\left[\exp\left\{ik\left(\frac{x_j^2}{2Z}\right)\right\}\right] \mathrm{E}\left[\exp\left\{ik\left(\frac{y_j^2}{2Z}\right)\right\}\right]\right|^2. \tag{12}$$

We can approximate

$$\begin{aligned}\mathrm{E}\left[\exp\left\{ik\left(\frac{x_j^2}{2Z}\right)\right\}\right] &= \int_{-L/2}^{L/2} f_X(x') \exp\left\{ik\left(\frac{x_j^2}{2Z}\right)\right\}\mathrm{d}x' \\ &\to \frac{1}{L}\int_{-\infty}^{\infty} \exp\left\{ik\left(\frac{x_j^2}{2Z}\right)\right\}\mathrm{d}x' = \frac{1}{L}\sqrt{\frac{i2\pi Z}{k}} \\ &= \frac{1}{L}\sqrt{i\lambda Z}. \end{aligned} \tag{13}$$

We end up with

$$\mathrm{E}[I(0,0,Z)] \sim \frac{(\lambda Z)^2}{L^4} N^2. \tag{14}$$

We have verified that the numerical are consistent with this estimate in the limit of high dipole density for a square emitting region. Adapting this formula to emission from a circular area by simply modifying the area appears to work well in comparison with numerical results.

4. Average Intensity in the Low Density Limit

We recall that the expectation value of the intensity is proportional to

$$\mathrm{E}[I(\mathbf{r})] \sim \sum_j \sum_{j'} \mathrm{E}\left[\exp\left\{ik(|\mathbf{r}-\mathbf{r}_j| - |\mathbf{r}-\mathbf{r}_{j'}|)\right\}\right]. \tag{15}$$

In the high density limit we took advantage of a Taylor series approximation, as well the separability of the sums in j and in j', to develop an estimate for the expectation value. In the low density limit it is possible to develop an estimate for the expectation value of the intensity by neglecting contributions from dipoles at different locations; at low density there are not nearby emitting dipoles for local phase coherence to contribute significantly. In this case we can write

$$\begin{aligned}\mathrm{E}[I(\mathbf{r})] &\sim \sum_j \mathrm{E}\left[\exp\left\{ik(|\mathbf{r}-\mathbf{r}_j| - |\mathbf{r}-\mathbf{r}_j|)\right\}\right] + \sum_j \sum_{j'\neq j} \mathrm{E}\left[\exp\left\{ik(|\mathbf{r}-\mathbf{r}_j| - |\mathbf{r}-\mathbf{r}_{j'}|)\right\}\right] \\ &= N + \sum_j \sum_{j'\neq j} \mathrm{E}\left[\exp\left\{ik(|\mathbf{r}-\mathbf{r}_j| - |\mathbf{r}-\mathbf{r}_{j'}|)\right\}\right] \to N. \end{aligned} \tag{16}$$

When the dipole density is low then the expectation value of the complex terms can be thought of as involving random phases so that

$$\mathrm{E}\left[\exp\left\{ik(|\mathbf{r}-\mathbf{r}_j|-|\mathbf{r}-\mathbf{r}_{j'}|)\right\}\right] \to \mathrm{E}\left[\mathrm{e}^{i\theta}\right] = \frac{1}{2\pi}\int_0^{2\pi}\mathrm{e}^{i\theta}\mathrm{d}\theta = 0.$$

In this limit there is no beam formation; instead there is a speckle pattern with average intensity proportional to N, in the vicinity of where a beam might have formed if N were higher, and also away from where the beam might have formed.

It is possible to develop an empirical approximation that includes both the contribution from the low density limit and from the high density limit according to

$$\mathrm{E}[I(\mathbf{r})] \sim \left|\sum_j \exp\left\{ik|\mathbf{r}-\mathbf{r}_j|\right\}\right|^2 = \begin{cases} N + \left(\dfrac{\lambda Z}{L^2}\right)^2 N^2, & \text{within beam pattern,} \\ N, & \text{outside of beam.} \end{cases} \tag{17}$$

This result is closely related to the exact formal result for the expectation value in [27,31].

5. Numerical Results

We have carried out simulations with randomly located dipoles in a square corresponding to the models described above, and have found good agreement with the simple probabilistic models outlined above. The exposed surface of the cathodes in the Karabut experiment are circular, which motivates us to consider the generalization

$$\mathrm{E}[I(\mathbf{r})] \sim \mathrm{E}\left[\left|\sum_j \exp\left\{ik|\mathbf{r}-\mathbf{r}_j|\right\}\right|^2\right] = \begin{cases} N + \left(\dfrac{\lambda Z}{\pi R^2}\right)^2 N^2, & \text{within beam pattern,} \\ N, & \text{outside of beam} \end{cases} \tag{18}$$

appropriate to emitting dipoles within a circular region of radius R.

An example of beam formation is illustrated in Fig. 2, where we see that dipoles randomly localized on a plane within a circle of radius 100 μm results in a circular beam with a radius 100 μm. Diffraction rings are apparent in the image which are a result of the discontinuity in the dipole density near the edge of the circular emitting area. One also sees a speckle pattern which results from the limited number of dipoles present in the calculation.

In Fig. 3 is shown the average intensity (from many simulations) in the case of a 100 μm radius circle containing random emitting dipoles and a 100 μm radius circle on the image plane displaced 25 cm in z. One can see that at low dipole density the average intensity is that of a spot pattern, and at high intensity the average intensity matches the analytic estimate. The empirical formula of Eq. (18) is seen to be a good match over the whole range of dipole densities.

6. Beam Formation in the Karabut Experiment

Although we have no published photographic record of beam formation in Karabut's experiment, there are two photographs that show the damage done to a Be window and a plastic window in [30]. It might have been possible to discern the amount of speckle present from an X-ray photographic image of the beam, which based on the analysis above would have provided us with information about how many emitting dipoles are present. In some of the photographic spectra taken in the bent mica crystal spectrometer configuration of Ref. [8] there is obvious speckle present,

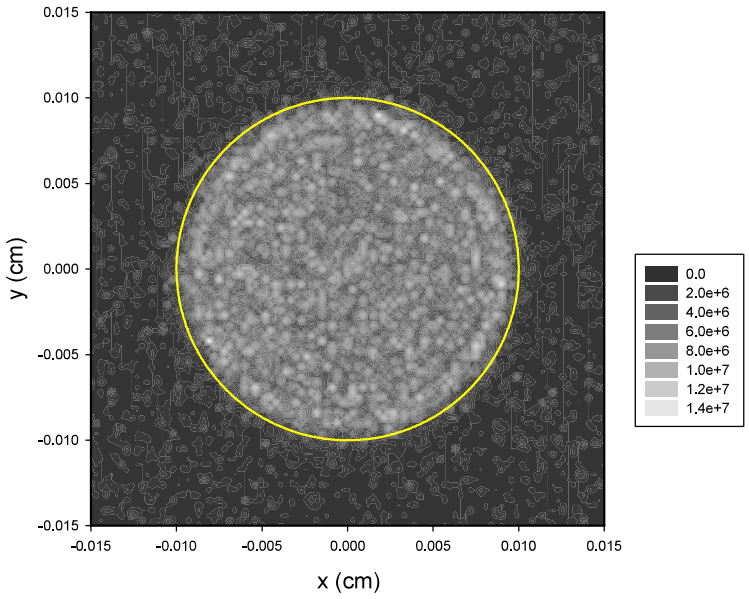

Figure 2. Beam at image plane located at $Z = 25$ cm in the case of a dipole density of 10^9 cm^{-2} localized in a circle of radius 100 μm. Marked in yellow is a circle of radius 100 μm.

which tells us that the quadratic beam contribution to the intensity is not so many orders of magnitude greater than the linear speckle contribution.

From the empirical model described above we can define a critical number of dipoles N_0 at which the linear and quadratic contributions match

$$N_0 = \left(\frac{\lambda Z}{\pi R^2}\right)^2 N_0^2. \tag{19}$$

We can evaluate

$$N_0 = \left(\frac{\pi R^2}{\lambda Z}\right)^2. \tag{20}$$

If we assume that phase coherence among the emitting dipoles is established over the entire surface of the cathode, then we can develop a numerical estimate for the critical number of dipoles. For this estimate we take

$$R = 0.5 \text{ cm}, \quad \lambda = 8 \text{ nm}, \quad Z = 25 \text{ cm}. \tag{21}$$

The corresponding critical number in this case is

$$N_0 = 1.5 \times 10^{11}. \tag{22}$$

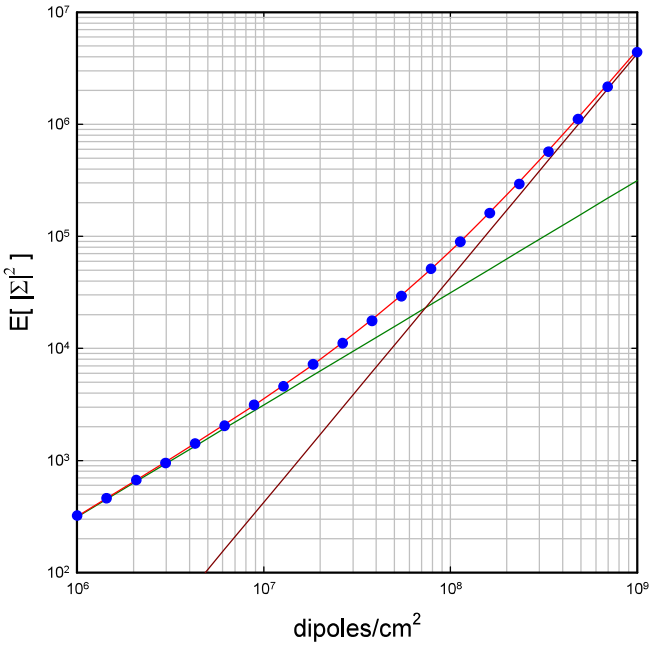

Figure 3. Expectation value $\mathrm{E}\left[\left|\sum_j \exp\left\{ik|\mathbf{r}-\mathbf{r}_j|\right\}\right|^2\right]$ as a function of dipole density (*red circles*); low density limit (*blue line*); high density limit (*dark green line*); empirical estimate (*dark green line*).

In this picture we would good expect beam formation when the number of dipoles is larger than N_0 by an order of magnitude or more.

Another possibility is that phase coherence is established over only a part of the cathode surface, in which case the critical number of dipoles would be smaller by the square of the ratio of the coherence area to the cathode area.

7. Spot Formation

When the dipole density is low we see speckle formation in the image plane, which is a consequence of fluctuations in the intensity. We are interested in the development of a model that we can use to estimate the intensity of a spot given the number of emitting dipoles in a given area.

We recall that the intensity is determined from the random locations of the dipoles according to

$$I(\mathbf{r}) \sim \left|\sum_j \exp\left\{ik|\mathbf{r}-\mathbf{r}_j|\right\}\right|^2 . \tag{23}$$

To form a spot we need for the phases associated with the different dipoles to be nearly the same. In this model we are specifically not interested the phase coherence associated with beam formation, in which the contribution from many

dipoles near a point add coherently. Instead we are interested in spot formation where the contribution from dipoles that are well separated combine randomly.

Since the contribution from each dipole is assumed to be equal in this model, the only difference in the contribution comes from the phase factor. If the dipole positions are random, then we might presume that the associated phases are random as well. Consequently, we might consider the simpler model defined by

$$\theta = \left| \sum_{j=1}^{N} \exp\left\{ i\phi_j \right\} \right|^2 = \sum_{j=1}^{N} \sum_{k=1}^{N} \exp\left\{ i(\phi_j - \phi_k) \right\}. \tag{24}$$

From numerical simulations, the associated probability distribution is exponential in θ according to

$$f_\Theta(\theta) \to \frac{1}{N} \exp\left\{ -\frac{\theta}{N} \right\}. \tag{25}$$

This result is consistent with a random walk model in two dimensions, and is well known in the literature in the context of speckle [32]. In the event that fewer than the critical number of dipoles emit in this model, then there is little or no beam apparent, but instead individual randomly positioned spots associated with speckle.

According to this model the average intensity will be proportional to N

$$\mathrm{E}[I] \sim \mathrm{E}[\theta] = N \tag{26}$$

with spots at higher intensity being rarer exponentially in the intensity. This result is consistent with the low dipole density model discussed briefly above, where

$$\mathrm{E}[I(\mathbf{r})] \sim \mathrm{E}\left[\left| \sum_j \exp\left\{ ik|\mathbf{r} - \mathbf{r}_j| \right\} \right|^2 \right] = N. \tag{27}$$

In Fig. 4 we show a calculated image of the weak beam and spots under conditions where the density of dipoles is lower, so that the total number of emitting dipoles is a bit less than the critical number. In this case the dipole density is 5×10^7 cm^{-2}, and the critical density needed for beam formation is about 7.4×10^7 cm^{-2}. A histogram of intensities for the speckle pattern and weak beam inside of the indicated circle is shown in Fig. 5, and is seen to be close to exponential consistent with the discussion above, and in this case the number of match dipoles in the circle is a reasonable match to the exponential fall off.

Karabut reported that the "diffuse" spectra that he observed appears when the discharge is running, and that the very intense "sharp" emission could be seen when the discharge was turned off suddenly [8]. In this case there is a large current spike (short in time) which accompanies the turning off of the current. Of interest is how this "sharp" emission might be interpreted. We previously proposed that this effect could be a result of Dicke superradiance from emitting dipoles in a localized region, where the emitting region was thought to be on the order of a square millimeter [33]. In the following section surface deformations will be considered, which will provide a superior interpretation.

We might have conjectured that the very intense spots might be a speckle effect under conditions where the individual dipole emission is stronger than in the case of beam formation. One argument against such a proposal is that individual speckles in this calculation are quite small, with a peak intensity only over a few microns by a few microns. The intense features in Karabut's data are much larger.

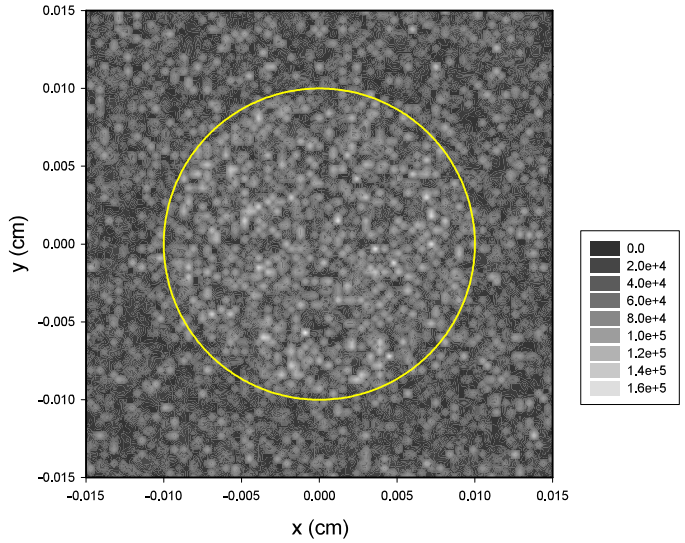

Figure 4. Beam at image plane (located at $Z = 25$ cm in the case of a dipole density of 5×10^7 cm^{-2} localized in a circle of radius 100 μm. Marked in yellow is a circle of radius 100 μm).

It is of interest to examine the intensity distribution in the case of beam formation. In Fig. 6 we show a histogram of the intensities when the emitting dipole density is 10^9 cm^{-2}. This intensity distribution corresponds to the beam illustrated in Fig. 2, which shows some diffraction rings inside near the boundary of the circle. The brightest speckles are seen to be associated with the outermost diffraction ring which is on average brightest. Once again the individual speckles in this calculation are very small, and we would not expect them to account for the intense spots seen in Karabut's experiment.

8. Surface Deformation Effects

After a number of runs in the glow discharge, the cathode has undergone plastic deformations (as was clear in experiments done at MIT with a copy of Karabut's system in the 1990s prior to the discovery of the collimated X-ray emission effect). Consequently, we would not expect there to be a mathematically flat surface present, even if the cathode somehow started out mathematically flat. There are also transient effects associated with compressional, transverse, and drum head mode excitation. We would expect the largest dynamic effects to be due to excitation of the drum head modes.

It is possible to include these effects in our description by working with a displacement field $\mathbf{u}(x,y,t)$ which keeps track of the amount of displacement in the different directions. The intensity pattern including surface displacement can be written as

$$I(\mathbf{r},t) \sim \left| \sum_j \exp\left\{ ik|\mathbf{r} - \mathbf{r}_j - \mathbf{u}(\mathbf{r}_j,t)| \right\} \right|^2 . \tag{28}$$

The idea here is that the dipole positions $\mathbf{r}_j$ are specified in the case of a mathematically flat surface. When the surface is displaced, the (slowly varying) displacement is added systematically to the initial positions of the dipoles in the contribution to the phase factors.

Since we expect the largest effect to come from drum head mode displacements and plastic deformations, we can restrict the surface displacement to be normal to the surface

$$\mathbf{u}(\mathbf{r},t) = \hat{\mathbf{i}}_z u(x,y,t). \tag{29}$$

It will be informative to consider the impact of low-order variations in the displacement; consequently, we work with a Taylor series expansion around the origin given by

$$u(x,y,t) = u(0,0,t) + x\frac{\partial u}{\partial x} + y\frac{\partial u}{\partial y} + \frac{1}{2}x^2\frac{\partial^2 u}{\partial x^2} + xy\frac{\partial^2 u}{\partial x \partial y} + \frac{1}{2}y^2\frac{\partial^2 u}{\partial y^2} + \cdots, \tag{30}$$

where the various derivatives are evaluated at $x = 0$ and $y = 0$, and may be oscillatory in time.

8.1. Uniform displacement

We consider first the impact of a uniform displacement

$$u(x,y,t) = u(0,0,t) = u_0(t). \tag{31}$$

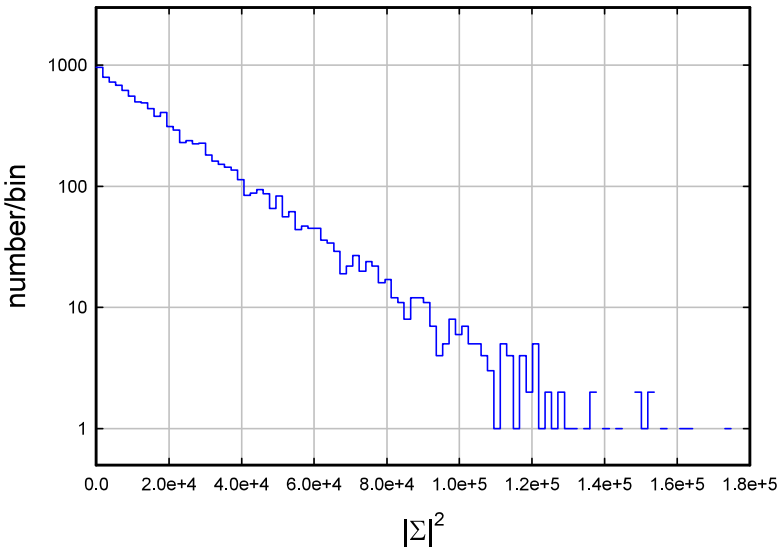

Figure 5. Histogram of intensity for speckle pattern with weak beam of Fig. 4.

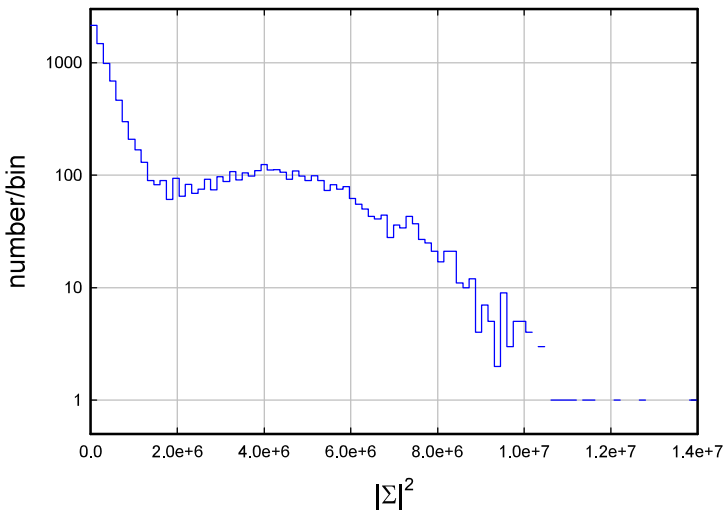

Figure 6. Histogram of intensity for speckle pattern with beam of Fig. 2 formed at an emitting dipole density of 10^9 dipoles/cm^2.

In this case we can write for the intensity

$$I(\mathbf{r},t) \sim \left| \sum_j \exp\left\{ ik|\mathbf{r} - \mathbf{r}_j - \hat{\mathbf{i}}_z u_0(t)| \right\} \right|^2$$
$$= \left| \sum_j \exp\left\{ ik\sqrt{(x-x_j)^2 + (y-y_j)^2 + (Z-u_0(t))^2} \right\} \right|^2 . \quad (32)$$

Since we expect the largest displacement to be very small compared to the distance between the cathode and image plane

$$|u_0(t)| \ll Z, \quad (33)$$

we do not anticipate observable effects from uniform surface displacements.

8.2. Linear displacements

Next we consider linear displacements of the form

$$u(x,y,t) = a(t)x + b(t)y. \quad (34)$$

In this case we can write

$$I(\mathbf{r},t) \sim \left| \sum_j \exp\left\{ ik\sqrt{(x-x_j)^2+(y-y_j)^2+[Z-a(t)x_j-b(t)y_j]^2} \right\} \right|^2 . \tag{35}$$

We would expect the beam to be offset (in the high dipole density limit) depending on the surface gradient. We can include this effect by writing

$$\begin{aligned} I(\mathbf{r}'(t),t) &= I(\mathbf{r}+\hat{\mathbf{i}}_x\delta x(t)+\mathbf{i}_y\delta y(t),t) \\ &\sim \left| \sum_j \exp\left\{ ik\sqrt{[x+\delta x(t)-x_j]^2+[y+\delta y(t)-y_j]^2+[Z-a(t)x_j-b(t)y_j]^2} \right\} \right|^2 . \end{aligned} \tag{36}$$

We can eliminate some of the low-order terms in the phase by choosing

$$\delta x(t) = -Za(t), \qquad \delta y(t) = -Za(t). \tag{37}$$

If we focus on the beam originally at the origin of the image plane then we can write

$$\begin{aligned} I(\hat{\mathbf{i}}_x\delta x(t)+\mathbf{i}_y\delta y(t),t) &\sim \left| \sum_j \exp\left\{ ik\sqrt{[\delta x(t)-x_j]^2+[\delta y(t)-y_j]^2+[Z-a(t)x_j-b(t)y_j]^2} \right\} \right|^2 \\ &= \left| \sum_j \exp\left\{ ik\sqrt{x_j^2+y_j^2+Z^2+\delta x(t)^2+\delta y(t)^2+[a(t)x_j+b(t)y_j]^2} \right\} \right|^2 . \end{aligned} \tag{38}$$

If the displacements are small, then the higher-order terms can be neglected, and we have the approximate result

$$I(\hat{\mathbf{i}}_x\delta x(t)+\mathbf{i}_y\delta y(t),t) \sim \left| \sum_j \exp\left\{ ik\sqrt{x_j^2+y_j^2+Z^2} \right\} \right|^2 . \tag{39}$$

In this approximation the beam is collimated normal to the displaced surface, which is mathematically flat but not in the $x-y$ plane. The neglected phase factors in this case are present since the image plane is not collinear with the displaced flat surface.

8.3. Surface curvature

If the surface is curved, there is the possibility of increasing or reducing the beam intensity, since it may be that phase coherence can be maintained for more emitting dipoles. In general we can describe a curved surface through displacements of the form

$$u(x,y) = c(t)x^2 + d(t)y^2 + f(t)xy. \tag{40}$$

In this case we can write

$$I(\mathbf{r},t) \sim \left| \sum_j \exp\left\{ ik \left| \mathbf{r} - \mathbf{r}_j - \hat{\mathbf{i}}_z [c(t)x_j^2 + d(t)y_j^2 + f(t)x_j y_j] \right| \right\} \right|^2$$
$$= \left| \sum_j \exp\left\{ ik \sqrt{(x-x_j)^2 + (y-y_j)^2 + [Z - c(t)x_j^2 - d(t)y_j^2 - f(t)x_j y_j]^2} \right\} \right|^2 . \quad (41)$$

The intensity at the origin reduces to

$$I(0,0,Z,t) \sim \left| \sum_j \exp\left\{ ik \sqrt{x_j^2 + y_j^2 + [Z - c(t)x_j^2 - d(t)y_j^2 - f(t)x_j y_j]^2} \right\} \right|^2 . \quad (42)$$

Note that it is possible to arrange for cancellation if

$$2Zc(t) = 1, \quad 2Zd(t) = 1, \quad f(t) = 0. \quad (43)$$

In this case we can write

$$I(0,0,Z,t) \sim \left| \sum_j \exp\left\{ ik \sqrt{Z^2 + \frac{(x_j^2 + y_j^2)^2}{4Z^2}} \right\} \right|^2$$
$$= \sum_j \sum_{j'} \exp\left\{ ik \left(\sqrt{Z^2 + \frac{(x_j^2 + y_j^2)^2}{4Z^2}} - \sqrt{Z^2 + \frac{(x_{j'}^2 + y_{j'}^2)^2}{4Z^2}} \right) \right\} . \quad (44)$$

We can make use of a Taylor series expansion in this case to write

$$\sqrt{Z^2 + \frac{\rho_j^4}{4Z^2}} - \sqrt{Z^2 + \frac{\rho_{j'}^4}{4Z^2}} = \frac{\rho_j^4 - \rho_{j'}^4}{8Z^3} + \cdots \quad (45)$$

The intensity in this limit is approximately

$$I(0,0,Z,t) \sim \sum_j \sum_{j'} \exp\left\{ ik \left(\frac{(x_j^2 + y_j^2)^2 - (x_{j'}^2 + y_{j'}^2)^2}{8Z^3} \right) \right\} . \quad (46)$$

It is probably simplest to evaluate the expectation value assuming N emitting dipoles in a circular area with radius ρ_0 around the origin, in which case the expectation value of the intensity is

$$\mathrm{E}[I(0,0,Z,t)] \sim \mathrm{E}\left[\sum_j \sum_{j'} \exp\left\{ik\left(\frac{(x_j^2+y_j^2)^2-(x_{j'}^2+y_{j'}^2)^2}{8Z^3}\right)\right\}\right]$$
$$= N^2\left|\mathrm{E}\left[\exp\left\{ik\left(\frac{\rho_j^4}{8Z^3}\right)\right\}\right]\right|^2. \tag{47}$$

To evaluate the expectation value we make use of a radial probability distribution given by

$$f(\rho) = \begin{cases} \dfrac{2\rho}{\rho_0^2}, & 0 \le \rho \le \rho_0, \\ 0, & \text{otherwise.} \end{cases} \tag{48}$$

We can compute

$$\mathrm{E}\left[\exp\left\{ik\left(\frac{\rho_j^4}{8Z^3}\right)\right\}\right] = \frac{2}{\rho_0^2}\int_0^{\rho_0} \rho \exp\left\{ik\left(\frac{\rho^4}{8Z^3}\right)\right\} \mathrm{d}\rho. \tag{49}$$

If the circle is sufficiently large, so that

$$\frac{k\rho_0^4}{8Z^3} = \frac{\pi\rho_0^4}{4\lambda Z^3} \gg 1 \tag{50}$$

(the characteristic value of ρ_0 for the numbers under consideration is about 2.5 mm) then we obtain

$$\mathrm{E}\left[\exp\left\{ik\left(\frac{\rho_j^4}{8Z^3}\right)\right\}\right] \to \frac{1}{\sqrt{-i}}\sqrt{\frac{2\pi Z^3}{k\rho_0^4}}. \tag{51}$$

In the end we can write

$$\mathrm{E}\left[\sum_j \sum_{j'} \exp\left\{ik\left(\frac{(x_j^2+y_j^2)^2-(x_{j'}^2+y_{j'}^2)^2}{8Z^3}\right)\right\}\right] = \left(\frac{2\pi Z^3}{k\rho_0^4}\right)N^2 = \left(\frac{\lambda Z^3}{\rho_0^4}\right)N^2. \tag{52}$$

This is a much greater intensity that we obtained with earlier models. Collimated X-ray emission under conditions where the surface is distorted in this way can result in a very intense beam with a corresponding small spot size at the image plane.

We note that surface displacement in this case is a focusing effect, with no enhancement in the area integral of the intensity at the image plane. An example of a focused beam with parameters

$$c(t) = 0.80\,\frac{1}{2Z}, \qquad d(t) = 0.80\,\frac{1}{2Z}, \qquad f(t) = 0 \tag{53}$$

is illustrated in Fig. 7. A beam in the shape of a line longer than the size of the circle containing the emitting dipoles is shown in Fig. 8. In this case the distorted surface parameters are

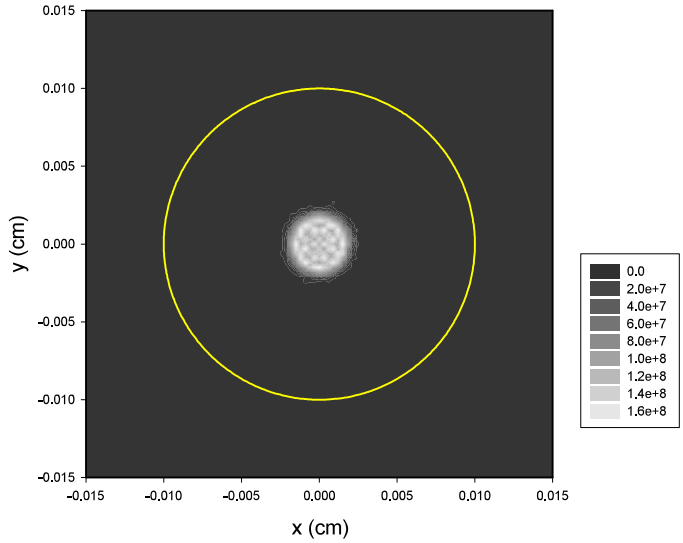

Figure 7. Partially focused beam at image plane located at $Z = 25$ cm in the case of a dipole density of 10^9 cm^{-2}. Marked in yellow is a circle of radius 100 μm.

$$c(t) = -0.30\,\frac{1}{2Z}, \qquad d(t) = 0.90\,\frac{1}{2Z}, \qquad f(t) = 0. \tag{54}$$

9. Discussion and Conclusions

Collimated X-ray emission in the Karabut experiment is an anomaly that cannot be understood based on currently accepted solid state and nuclear physics, which provides motivation for seeking an understanding of the effect. There are two possible origins of a collimation effect: either an X-ray laser has been created; or else beam formation is due to phased array emission. We have argued many times against the proposal that an X-ray laser has been created, in part due to the absence of any compelling mechanism to produce a population inversion, in part due to the associated high power density requirement, and in part due to the mismatch between the geometry needed for beam formation and the geometry of the experiment.

Instead we have conjectured that the collimation is a consequence of phased array emission, a proposal which on the one hand is free of the strong objections against an X-ray laser mechanism, but which on the other hand brings new issues to resolve. The two most significant mechanistic issues are how excitation in the keV range can be produced, and how phase coherence might be established. These problems are very serious; however, in our view there are plausible mechanisms for both of these issues.

Independent of Karabut's experiment we have for many years been interested in mechanisms that might down-convert a large nuclear quantum in the Fleischmann–Pons experiment, to account for excess heat as due to nuclear reactions without commensurate energetic nuclear radiation. The big headache in understanding the mechanism through which excess heat is produced is that in a successful experiment one has the possibility of measuring thermal energy and ^{4}He in the gas phase, neither of which at this point shed much light on whatever physical mechanism is involved.

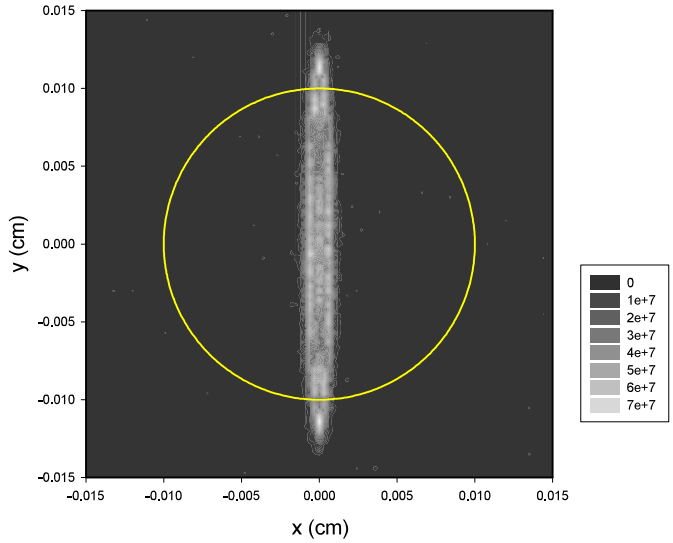

Figure 8. Beam partially focused in x and defocused in y at image plane located at $Z = 25$ cm in the case of a dipole density of 10^9 cm^{-2}. Marked in yellow is a circle of radius 100 μm.

If the large nuclear quantum is being down-converted, then we would want to study the down-conversion mechanism in a different kind of experiment more easily diagnosed and interpreted. Because of the intimate theoretical connection between up-conversion and down-conversion, we have the possibility of understanding how down-conversion works by studying up-conversion. Initially we contemplated a theory-based experiment in which THz vibrations would be up-converted to produce excitation at 1565 eV in ^{201}Hg nuclei, which has the lowest energy excited state of all the stable nuclei, and which would decay primarily by internal conversion but also in part via X-ray emission. In this proposed theory-based experiment we recognized that the up-conversion of vibrational energy would result in phase coherence, with the possibility of phased array beam formation. The claim of collimated X-ray emission near 1.5 keV in the Karabut experiment drew our attention since it seemed that the up-conversion experiment that we were interested might have already been implemented. From this perspective collimation in the Karabut experiment could be interpreted as an experimental confirmation of the up-conversion mechanism, primarily since there seems to be no other plausible interpretation. Collimated X-ray emission claimed in some cases near 1.5 keV in the water jet experiments of Kornilova, Vysotskii and coworkers [34–37] seems to us to be closely related, and to provide another experiment where up-conversion is observed (a point of view we note that is at odds with the theoretical explanation put forth by Vysotskii in these references).

One motivation for the modeling described in this paper was to see whether we might develop constraints on the number of emitting dipoles involved, which according to our picture would shed light on the number of mercury atoms present on the surface. We had thought initially that low levels of mercury as an impurity in the cathodes or in the gas might be responsible for the collimated emission; however, the spectra published by Karabut shows no indication of edge absorption which favors implantation from mercury contamination in the discharge gas. For example, the K-edge absorption in aluminum starts at 1562 eV, which should be readily apparent if the emission originates in the bulk. The transmission for a 1 μm Al layer is close to 90% below the K-edge, and near 30% above the K-edge (see

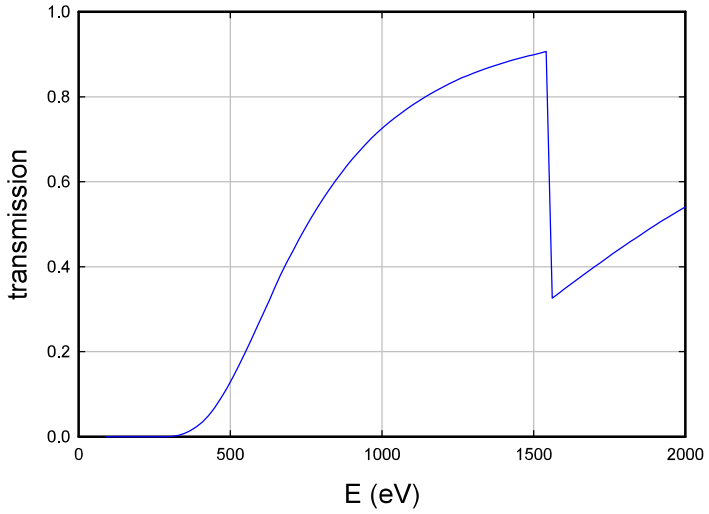

Figure 9. Transmission through 1 μm of Al as a function of the X-ray energy from Henke's online x-ray transmission calculator.

Fig. 9); this difference would be readily apparent in the spectra if the emission was due to bulk radiators. The absence of an observable K-edge absorption feature in the spectrum suggests that the emission is localized to within 0.1 μm or less from the surface, which is consistent with implantation from the mercury as an impurity in the discharge gas. Beam formation requires a dipole density above a threshold value, and we have estimated the threshold to correspond to about 1.5×10^{11} emitting dipoles in the Karabut experiment. Probably the total number of dipoles is on the order of 1.5×10^{12} or higher, to be consistent with unambiguous beam formation. Since the natural abundance of ^{201}Hg is 13.18%, this puts the total number of mercury atoms at or above 10^{13}.

For beam formation we made use of a model based on emitting dipoles randomly positioned on a mathematical plane within a circle, to match the cathode geometry in Karabut's experiment. Beam formation in this case requires both uniform phase, and for there to be a mathematical plane to restrict random variations in position normal to the surface. In previous work presented at ICCF17 we assumed that the dipoles were randomly spaced in a volume near the surface, which could produce speckles, but we did not appreciate at the time that this model does not produce a beam of about the same size as the cathode. The orientation of the crystal planes aligned with the surface produced by the rolling process used in the fabrication of the foils from which the cathodes are taken is critical for beam formation, based on the model studied in this paper.

We have speculated previously about the origin of the very intense spots and lines that appear on the film (and which produces film damage), including proposals that small fraction of the surface produces a collimated beam to form a spot, and that a line might be produced by a steering effect. Here we have shown that surface deformation can produce a focusing of the beam, both in one dimension to produce a line, and in two dimensions to produce a spot. This new picture provides in our view a much stronger argument than the earlier speculation.

We have previously speculated at ICCF17 that the bursts in emission following the turning off of the discharge was due to nonlinear Rabi oscillations in the donor and receiver model, a proposal strongly criticized by Vysotskii [38] on the grounds that the strong coupling needed to produce such rapid nonlinear Rabi oscillations was unlikely. In

retrospect Vysotskii's argument seems right, and we have subsequently been thinking about new models for the up-conversion which will be discussed elsewhere. However, in these models the burst effect comes about from the basic time dependence of the phonon–nuclear coupling matrix element, which in this case involves two photon exchange since the transition is M1 and the phonon-nuclear interaction is E1, to produce a $\cos^4 \omega_0 t$ time-dependence which is sharpened by a nonlinearity associated with local up-conversion effects. In this picture the excitation of the ^{201}Hg transition is from excitation transfer from much more strongly coupled transitions in the cathode holder and steel target chamber, and drum head mode excitation of the cathode mediates this excitation transfer.

References

[1] A.B. Karabut, Ya.R. Kucherov and I. B. Savvatimova, Nuclear product ratio for glow discharge in deuterium, *Phys. Lett. A.* **170** (1992) 265–272.

[2] A.B. Karabut, Research into powerful solid X-ray laser (wave length is 0.8–1.2 nm) with excitation of high current glow discharge ions, *Proc. 11th Int. Conf. on Emerging Nuclear Energy Systems*, 29 September–4 October 2002, Albuquerque, New Mexico, USA, pp. 374–381.

[3] A.B. Karabut, Experimental research into characteristics of X-ray emission from solid-state cathode medium of high-current glow discharge, *Proc. 10th Int. Conf. on Cold Fusion*, August 24–29, 2003, Cambridge, MA, USA.

[4] A.B. Karabut, Research into characteristics of X-ray emission laser beams from solid-state cathode medium of high current glow discharge, *Proc. 11th Int. Conf. on Cold Fusion*, 31 October–5 November, 2004, France, pp. 253–257.

[5] A.B. Karabut, Study of energetic and temporal characteristics of X-ray emission from solid state cathode medium of high current glow discharge, *Proc. 12th Int. Conf. on Cold Fusion*, December 2–7, 2006, Japan, pp. 344–350.

[6] A.B. Karabut and E.A. Karabut, Research into energy spectra of X-ray emission from solid cathode medium during the high current glow discharge operation and after the glow discharge current switch off, *Proc. 14th Int. Conf. on Cold Fusion*, August 10–15, 2008, USA.

[7] A.B. Karabut and E.A. Karabut, Study of deuterium loading into Pd cathode samples of glow discharge, *Proc. 9th Int. Workshop on Anomalies in Hydrogen/Deuterium Gas Loaded Metals*, 6–11 September 2010, Siena, Italy.

[8] A.B. Karabut, E.A. Karabut and P.L. Hagelstein, Spectral and temporal characteristics of X-ray emission from metal electrodes in a high-current glow discharge, *J. Condensed Matter Nucl. Sci.* **6** (2012) 217.

[9] A.B. Karabut and E.A. Karabut, Research into excited 0.6–6.0 keV energy levels in the cathode solid medium of glow discharge by X-ray spectra emission, *J. Condensed Matter Nucl. Sci.* **8** (2012) 159.

[10] A.B. Karabut, Research into excited long lived 0.6–6.0 keV energy levels in the cathode solid medium of glow discharge by X-ray spectra emission, *J. Materials Sci. Eng. B* **3** (2013) 298.

[11] B.I. Ivlev, X-ray laser pulses from solids, *arXiv preprint* arXiv:1512.08504 (2015).

[12] B.I. Ivlev, Conversion of zero point energy into high-energy photons, *Revista Mexicana de Física* **62** (2016) 83–88.

[13] P.L. Hagelstein, Physics of short-wavelength-laser design, Ph.D. Thesis, MIT, 1981.

[14] P.L. Hagelstein and I.U. Chaudhary. Phonon models for anomalies in condensed matter nuclear science, *Current Sci.* **108** (2015) 507.

[15] P.L. Hagelstein, Directional X-ray and gamma emission in experiments in condensed matter nuclear science, *Current Sci.* **108** (2015) 601.

[16] P.L. Hagelstein, Current status of the theory and modeling effort based on fractionation, *J. Condensed Matter Nucl. Sci.* **19** (2016) 98–109.

[17] I.L. Dillamore and W.T. Roberts, Preferred orientation in wrought and annealed metals, *Metallurgical Rev.* **10** (1965) 271–380.

[18] R. Gotthardt, G. Hoschek, O. Reimold and F. Haessner, Topographic arrangement of crystallite orientations in rolled copper, *Texture* **1** (1972) 99–109.

[19] H. Hu, Texture of metals, *Texture* **1** (1974) 233–258.

[20] Y. Lo, A mathematical theory of antenna arrays with randomly spaced elements, *IEEE Trans. Antennas and Propagation* **12** (1964) 257–268.

[21] V.D. Agrawal and Y.T. Lo, Distribution of sidelobe level in random arrays, *Proc. IEEE* **57** (1969) 1764–1765.
[22] B. Steinberg, The peak sidelobe of the phased array having randomly located elements, *IEEE Trans. Antennas and Propagation* **20** (1972) 129–136.
[23] M. Donvito and S. Kassam, Characterization of the random array peak sidelobe, *IEEE Trans. Antennas and Propagation* **27** (1979) 379–385.
[24] H. Ochiai, P. Mitran, H.V. Poor and V. Tarokh, Collaborative beamforming in ad hoc networks, *Information Theory Workshop* IEEE (2004) 396–401.
[25] N.N. Ma, K. Buchanan, J. Jensen and G. Huff, Distributed beamforming from triangular planar random antenna arrays, *Military Commun. Conf. MILCOM*, IEEE (2015) 553–558.
[26] J.V. Thorn, N.O. Booth and J.C. Lockwood, Random and partially random acoustic arrays, *J. Acoustical Soc. Amer.* **67** (1980) 1277–1286.
[27] W.S. Hodgkiss, Random acoustic arrays, *Underwater Acoustics and Signal Processing*, Springer Netherlands, 1981, pp. 327–338.
[28] K.R. Buchanan, Theory and applications of aperiodic (random) phased arrays, Ph.D. dissertation, Texas A&M University, 2014.
[29] J.D. Jackson, *Classical Electrodynamics*, Wiley, New York, 1975.
[30] A.B. Karabut, X-ray emission in the high current density glow discharge experiments, *Proc. ICCF9* (2002) 155–158.
[31] D.H. Johnson and D.E. Dudgeon, *Array Signal Processing*, Prentice-Hall, Upper Saddle River, NJ, 1993. See Section 3.3.6 on Random Arrays.
[32] J.W. Goodman, Some fundamental properties of speckle, *J. Optical Soc. Amer.* **66** (1976) 1145–1150.
[33] P.L. Hagelstein and I.U. Chaudhary, A model for collimated X-ray emission in the Karabut experiment, *Proc. ICCF17* (2013).
[34] A.A. Kornilovaa, V.I. Vysotskii, N.N. Sysoev, N.K. Litvin, V.I. Tomak and A.A. Barzov, Shock cavitational mechanism of X-ray generation during fast water stream cavitation, *Moscow University Physics Bulletin* **65** (2010) 46.
[35] A.A. Kornilova, V.I. Vysotskii, N. N. Sysoev, N.K. Litvin, V.I. Tomak and A.A. Barzov, Generation of intense X-rays during ejection of a fast water jet from a metal channel to atmosphere, *J. Surface Investigation. X-ray, Synchrotron and Neutron Techniques* **4** (2010)1008.
[36] V.I. Vysotskii, A.A. Kornilova, A.O. Vasilenko and V.I. Tomak, Detection and investigation of undamped temperature waves excited under water jet cavitation, *J. Surface Investigation. X-ray, Synchrotron and Neutron Techniques* **8** (2014) 1186–1192.
[37] V.I. Vysotskii, A.A. Kornilova and A.O. Vasilenko, Observation and investigation of anomalous X-ray and thermal effects of cavitation, *Current Sci.* **108** (2015) 608.
[38] V.I. Vysotskii, private communication.